



## RESEARCH ARTICLE

# A fluorinated phosphite traps alkoxy radicals photogenerated at the air/solid interface of a nanoparticle

Goutam Ghosh<sup>1,2</sup> | Alexander Greer<sup>1,2</sup> <sup>1</sup>Department of Chemistry, Brooklyn College, Brooklyn, New York, USA<sup>2</sup>Ph.D. Program in Chemistry, The Graduate Center of the City University of New York, New York, New York, USA**Correspondence**Alexander Greer, Department of Chemistry, Brooklyn College, 2900 Bedford Avenue, Brooklyn, New York, NY 11210, USA.  
Email: agreer@brooklyn.cuny.edu**Funding information**

National Science Foundation, Grant/Award Number: CHE-1856765

**Abstract**

With interests in alkoxy radical formation on natural and artificial surfaces, a physical-organic study was carried out with a Hammett series of triaryl phosphites (*p*-MeO, H, *p*-F, and *p*-Cl) to trap adsorbed alkoxy radicals on silica nanoparticles. A mechanism which involves PhC (Me)<sub>2</sub>O• and EtO• trapping in a cumylethyl peroxide sensitized homolysis reaction is consistent with the results. The *p*-F phosphite was able to indirectly monitor the alkoxy radical formation, and <sup>31</sup>P NMR readily enabled this exploration, but other phosphites of the series such as the *p*-MeO phosphite were limited by hydrolysis reactions catalyzed by surface silanol groups. Fluorinated silica nanoparticles helped to suppress the hydrolysis reaction although adventitious water also plays a role in hindering efficient capture of the alkoxy radicals by the phosphite traps.

**KEYWORDS**

alkoxy radicals, nanoparticles, phosphite traps, photosensitization, reactive intermediates

## 1 | INTRODUCTION

There are difficulties in assessing surface effects on alkoxy radicals and knowing the difference they may display at the air/solid interface in the absence of solvent. Some challenges have been surmounted with the use of EPR. For example, in 1994, Forbes et al. reported on a time-resolved EPR study of organic radicals anchored to silica surfaces to probe their magnetic and kinetic properties at the solution/solid interface.<sup>[1–3]</sup> A unique facet of this study was observations of stronger spin polarizations in radical pairs tethered closely to the surface which disappeared in longer tethers, where radical pairs behave similarly to those in free solution. Norrish type I cleavage was used as a means to study the biradicals after decarbonylation and surface phenomena on these silica particles.<sup>[2]</sup>

Natural and artificial particles have been reported to bear surface radicals, in some instances persistent radicals,<sup>[4–9]</sup> where EPR is often used. Thus, there is a need for additional trapping methods for radicals on

surfaces, which we carry out here with triaryl phosphites on silica particles, where <sup>31</sup>P NMR is used.

Here, we use *p*-substituted aryl phosphites as traps with potential alkoxy radical scavenging activity, due to their oxophilic phosphorus atoms (Figure 1). The trapping of cumyloxy and ethoxy radicals generated by the photosensitization of cumylethyl peroxide **2** was investigated with four phosphites, (*p*-X-C<sub>6</sub>H<sub>4</sub>-O)<sub>3</sub>P [X = OMe (**3a**), H (**3b**), F (**3c**), and Cl (**3d**)]. Our method is indirect and uses product identification to quantitate alkoxy radical formation at the air/silica interface. Dione **1**, cumylethyl peroxide **2**, and a Hammett series of triaryl phosphites were adsorbed on silica in N<sub>2</sub>-degassed vessels, in which **1** was irradiated with (280 < λ < 700 nm) light. This Hammett study of a series of triaryl phosphites provide an approach to the study of alkoxy radicals on non-porous nanoparticle surfaces. After photolysis or heating, the compounds were desorbed from the fumed silica surface, and <sup>31</sup>P NMR was used to quantitate the products formed.

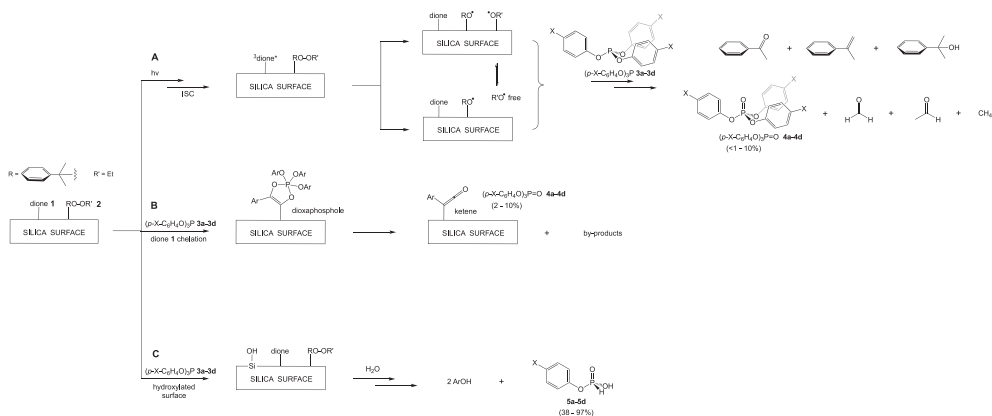


**FIGURE 1** Proposed paths (A-C) for photochemical and thermal reactions of 4,4'-dimethylbenzil (dione) **1** and cumylethyl peroxide **2** at the gas/silica interface probed by triaryl phosphite trapping agents. A Hammett series of *p*-substituted triaryl phosphites ( $p$ -X-C<sub>6</sub>H<sub>4</sub>-O)<sub>3</sub>P [X = OMe (**3a**), H (**3b**), F (**3c**), or Cl (**3d**)] was used to probe the formation of triaryl phosphates ( $p$ -X-C<sub>6</sub>H<sub>4</sub>-O)<sub>3</sub>P=O **4a-4d**, aryl hydrogen phosphonates ( $p$ -X-C<sub>6</sub>H<sub>4</sub>-O)P(=O)OH **5a-5d**, and by-products

As we will see, the results show that the *tris*(4-F-phenyl) phosphite yielded alkoxy radical scavenging activity. In contrast, the hydrolysis on silica points to the more nucleophilic phosphites undergoing protonation and acceleration in aryl hydrogen phosphonate formation. The implications for the competition between phosphite's alkoxy radical scavenging and conversion to aryl hydrogen phosphonate as a function of surface conditioning (i.e., removal of SiOH sites by fluorination) are discussed. Interestingly, the phosphite hydrolysis leads to phenol derivatives, which themselves bear antioxidant character and will be discussed.

## 2 | RESULTS AND DISCUSSION

Native silica particles or fluorinated particles were adsorbed with dione **1** (0.01 mmol/g silica), cumylethyl peroxide **2** (0.1 mmol/g silica), and triaryl phosphites (in pairs of **3a** and **3b**, or **3b** and **3c**, or **3b** and **3d**) (each 0.1 mmol/g silica) in a N<sub>2</sub>-degassed vessel and irradiated with (280 < λ < 700 nm) light, or maintained at room temperature (25°C) or heated to 35°C. Each reaction was carried out for 1 h. Compounds were then desorbed from the silica particles with a polar solvent and the product ratios measured by <sup>31</sup>P NMR. The experimental evidence supports the mechanism in Figure 1, which has three paths (paths A-C), as we will discuss next.

### 2.1 | Path A. Interaction of RO• with aryl phosphites at the air/particle interface

We carried out the reaction of dione **1** and cumylethyl peroxide **2** in the presence of aryl phosphites on native

and fluorinated silica (Figure 2). After desorption from the particles, the percent yields of products were determined by <sup>31</sup>P NMR (Table 1). A control photoreaction study with dione **1** and phosphites **3a-3d**, with no peroxide **2** present showed that the percent phosphate formed was 0% on native silica and 0-3% on fluorinated silica. The percent of phosphate formed is dependent on light and the photosensitized generation of alkoxy radicals. Photons from the light source (280 < λ < 700 nm) are mainly absorbed by 4,4'-dimethylbenzil **1** due to its ~10-fold greater absorption in the blue region at 280 nm than the phosphites. The irradiation of dione **1**, peroxide **2** and phosphites **3a-3d**, increased the percent yield of phosphate up to 10%. We attribute the increase to the interaction of RO• and R'O• with the phosphites on the native and fluorinated silica particles. However, the alkoxy radical trapping by phosphites was relatively low yielding for **3c** (X = F, 7-10%) and **3d** (X = Cl, 1-2.5%) and yielded no phosphate for **3a** (X = OMe, 0%) and **3b** (X = H, 0%). As we will show later, the absence of alkoxy radical activity of phosphites (X = OMe and H) is due to their consumption (i.e., loss) by surface hydrolysis to aryl hydrogen phosphonates. Another kind of loss involves the lower molecular weight R'O•, which is not easily detected in the headspace of the air/solid experiment, but is detected in a homogeneous reaction in CD<sub>3</sub>CN as downstream products CH<sub>4</sub> and MeCHO (Figure S6, see the Supporting Information section). Intermolecular and intramolecular reactions<sup>[10,11]</sup> of the higher molecular weight RO• takes place, where we also detect cumyl alcohol, β-methylstyrene, and acetophenone. Next, we examined the alkoxy radical trapping in connection (and competition) with a chelation reaction.

**FIGURE 2** Reactions of  $\text{PhC}(\text{Me})_2\text{O}\cdot$  and  $\text{EtO}\cdot$  radicals with triaryl phosphite traps and other conversions to products (path A)

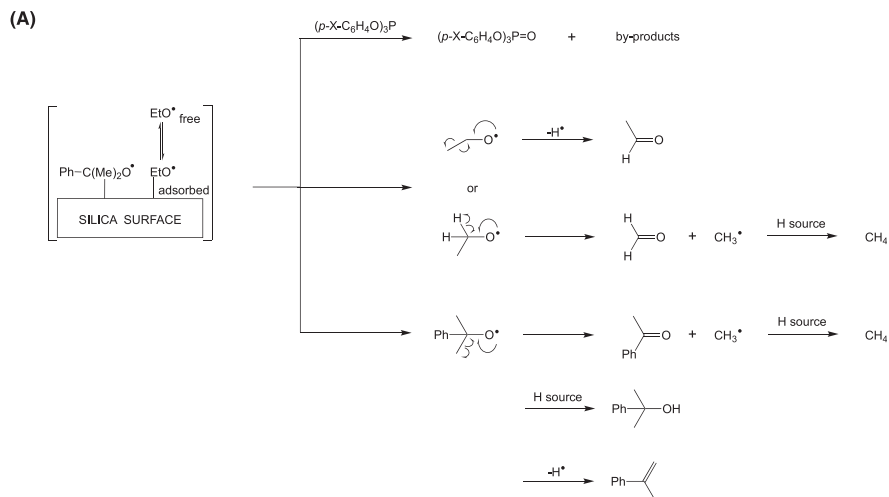


**TABLE 1** Triaryl phosphate **4a-4d** percent yield measurements in photosensitized or heated reactions of dione **1**, cumylethyl peroxide **2**, and  $(p\text{-X-C}_6\text{H}_4\text{-O})_3\text{P}$  **3a-3d** on native and fluorinated silica nanoparticles<sup>a,b</sup>

Entry	Phosphite ( $p\text{-X-C}_6\text{H}_4\text{-O}$ ) <sub>3</sub> P	Dione 1: Peroxide 2: Phosphite ratio	Phosphate <b>4a-4d</b> formed upon irradiation [path A (%)] <sup>c,d</sup>		Phosphate <b>4a-4d</b> formed by heating to 35°C [path B (%)] <sup>c,d</sup>		Phosphate <b>4a-4d</b> formed by irradiation and heat [paths A + B (%)] <sup>c,d</sup>	
			SiO <sub>2</sub>	F-SiO <sub>2</sub>	SiO <sub>2</sub>	F-SiO <sub>2</sub>	SiO <sub>2</sub>	F-SiO <sub>2</sub>
1	X = OMe <b>3a</b>	1:10:10	0	0	2	9.5	2	9.5
2	X = H <b>3b</b>	1:10:10	0	0	6.5	7	6.5	7
3	X = F <b>3c</b>	1:10:10	10	7	10	10	20	17
4	X = Cl <b>3d</b>	1:10:10	1	2.5	10	10	11	12.5

<sup>a</sup>Dione **1** (0.01 mmol/g silica), **2** (0.1 mmol/g silica), and **3a-3d** (in pairs with each 0.1 mmol/g silica) were adsorbed on native silica (SiO<sub>2</sub>) or fluorinated silica (F-SiO<sub>2</sub>) (0.2 g) and irradiated or heated.

<sup>b</sup>Samples were irradiated with (280 < λ < 700 nm) light or heated to 35°C.

<sup>c</sup>The triaryl phosphates **4a-4d** were detected by <sup>31</sup>P NMR. The data are the average of two runs with ±10-15% error.

<sup>d</sup>The percent yields of triaryl phosphates **4a-4d** were based on their integrated peak areas without the use of an external standard.

## 2.2 | Path B. Competing alkoxy radical trapping and chelation of phosphites at a silica surface: More than one way to the phosphate products

The reaction of dione **1** (an α-diketone) and phosphites **3a-3e** was followed in the formation of phosphates **4a-4e** on the native and fluorinated silica particles (Table 1, path B). After 1 h at 25°C (in subdued room light), the percent yields of phosphates **4a-4e** on the fluorinated silica ranged from 0 to 3%. The percent phosphate formed was found to be dependent on heating of the sample. After 1 h at 35°C, the yields of phosphates **4a-4e** on the fluorinated surface increased and ranged from 7 to 10%. The yield in the latter can be rationalized by the encounter of dione **1** and phosphite in equimolar amounts.

The data are rationalized by suggesting the interaction of phosphite and dione **1** leads to a 2,2,2-triaryloxy-1,3,2λ<sup>5</sup>-dioxaphosphole intermediate (Figure 3). The chelation is a straightforward to the formation of the dioxaphosphole, and is expected to react further by an intramolecular migration of the *p*-tolyl group to reach the ketene [2,2-bis(*p*-tolyl)ethen-1-one] and triaryl phosphate [(*p*-X-C<sub>6</sub>H<sub>4</sub>-O)<sub>3</sub>P=O]. The source of triaryl phosphate was examined, in which the chelation of the phosphite relies on the conversion of the *trans*-dione **1** to the reactive *syn*- or *syn*-skewed-dione **1** conformer.<sup>[12]</sup> The results in path B supplement others<sup>[13-16]</sup> and our<sup>[12]</sup> previous work on phosphite chelation of diones and the NMR detection of the transient dioxaphosphole. Conceivable by-products are also α-hydroxyvinyl phosphates, but were not detected by NMR. While this experimental

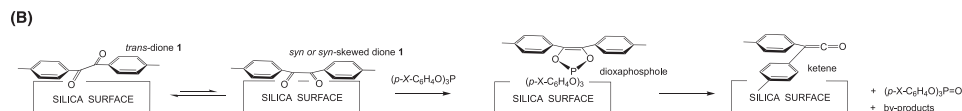


**FIGURE 3** Chelation of phosphites with dione **1** on the silica surface (path B)

method led to the production of ketene, it was not exploited for studies of ketenes at the air/solid surface.

### 2.3 | Path C. Surface effects and substituent effects on the hydrolysis of triaryl phosphites

Next, we sought to determine whether surface effects and the *tris*(4-*X*-phenyl) electronic effects are relevant in the hydrolysis of the triaryl phosphites. As is shown in Table 2, both play a role. Upon heating the sample to 35°C, the formation of aryl hydrogen phosphonates **5a–5d** was observed by <sup>31</sup>P NMR and detected in varying percent yields. On native silica, the aryl hydrogen phosphonate was the major product ranging from a high of 97% for **5a** to a low of 38% for **5d**. This percent yield decreased on fluorinated silica, ranging from a high of 30% for **5a** to a low of 0% for **5d**. Path C in Figure 4 shows a proposed mechanism for a surface acid catalyzed hydrolysis of the phosphites to reach aryl hydrogen phosphonates and *p*-substituted phenols. The proposed mechanism is similar to previous reports on phosphite hydrolysis.<sup>[17,18]</sup> The hydrolysis is thought to proceed

through the diaryl phosphinic acid and cease at aryl hydrogen phosphonate yielding two equivalents of the *p*-substituted phenol. The reaction does not continue further to produce phosphoric acid and a third mole of *p*-substituted phenol. The importance of electronic interactions of the (*p*-*X*-C<sub>6</sub>H<sub>4</sub>-O)<sub>3</sub>P compounds is also observed by a Hammett plot of log *k<sub>X</sub>/k<sub>H</sub>* vs  $\sigma_p$  to give a reaction constant  $\rho$  of  $-1.25$  on native silica and  $\rho$  of  $-2.34$  on fluorinated silica (Figure 5). Even though the  $\rho$  value on fluorinated silica is greater, the hydrolytic reactivity of the aryl phosphites is significantly higher on native silica. In the case of fluorinated silica, the Hammett series of triaryl phosphites function as nucleophiles, but with surface-adsorbed water as the proton source instead of silanols, as the silanols have been replaced with fluorosilanols.

### 3 | MECHANISM

We took advantage of a photosensitized homolysis of PhC(Me<sub>2</sub>)COOEt to reach RO• and R'O• radicals [R = C(Me<sub>2</sub>)Ph; R' = Et] and probe their reactivity at the air/solid interface with phosphite trapping agents (**3a–3d**). The trapping of the alkoxy radicals afforded phosphates, although it was not determined whether the RO• and R'O• are in competition with the (*p*-*X*-C<sub>6</sub>H<sub>4</sub>-O)<sub>3</sub>P traps as some R'O• may volatilize away from the surface and escape capture under our conditions. However, in a homogeneous experiment, the detection of trace CH<sub>4</sub> and MeCHO point to the intermediacy of CH<sub>3</sub>•, EtO•, and Ph(Me<sub>2</sub>)CO•, and the idea that these radicals undergo H-atom transfer reactions.<sup>[19–21]</sup>

The relatively small amount of phosphate formed in the photolysis of dione **1**, peroxide **2**, and (*p*-*X*-C<sub>6</sub>H<sub>4</sub>-O)<sub>3</sub>P makes a mechanistic study of surface-bound alkoxy radicals challenging. The *p*-F phosphite **3c** revealed the highest trapping yield of alkoxy radicals with 10% *p*-F phosphate **4c**. Our results are not contrary to the expected electrophilicity of alkoxy radicals<sup>[22]</sup> due to their ease in forming an alkoxide anion upon accepting an electron rather than oxylum ion (RO<sup>+</sup>) by electron loss. Instead, the surface SiOH groups accounts for the ability of the *p*-F phosphite **3c** to monitor the alkoxy radical formation, but not other phosphites in the series such as the *p*-MeO phosphite **3a**, in which surface effects are less important for H-atom transfer compared to Brønsted acidity.

**TABLE 2** Aryl hydrogen phosphonate **5a–5d** percent yield measurements in photosensitized or heated reactions of dione **1**, cumylethyl peroxide **2**, and (*p*-*X*-C<sub>6</sub>H<sub>4</sub>-O)<sub>3</sub>P **3a–3d** on native and fluorinated silica nanoparticles<sup>a,b</sup>

Entry	Phosphite ( <i>p</i> - <i>X</i> -C <sub>6</sub> H <sub>4</sub> -O) <sub>3</sub> P	Dione <b>1</b> : Peroxide <b>2</b> : Phosphite ratio	Phosphonate <b>5a–5d</b> yield [path C (%)] <sup>c,d</sup>	
			SiO <sub>2</sub>	F-SiO <sub>2</sub>
1	X = OMe <b>3a</b>	1:10:10	97	30
2	X = H <b>3b</b>	1:10:10	76	6
3	X = F <b>3c</b>	1:10:10	43	5.5
4	X = Cl <b>3d</b>	1:10:10	38	0

<sup>a</sup>Dione **1** (0.01 mmol/g silica), **2** (0.1 mmol/g silica), and **3a–3d** (in pairs with each 0.1 mmol/g silica) were adsorbed on native silica (SiO<sub>2</sub>) or fluorinated silica (F-SiO<sub>2</sub>) (0.2 g) and irradiated or heated.

<sup>b</sup>Samples were heated to 35°C.

<sup>c</sup>The aryl hydrogen phosphonates **5a–5d** were detected by <sup>31</sup>P NMR. The data are the average of two runs with  $\pm 10$ –15% error.

<sup>d</sup>The percent yields of aryl hydrogen phosphonates **5a–5d** were based on their integrated peak areas without the use of an external standard.

**FIGURE 4** Triaryl phosphite hydrolysis and the formation of aryl hydrogen phosphonate and phenol (path C)

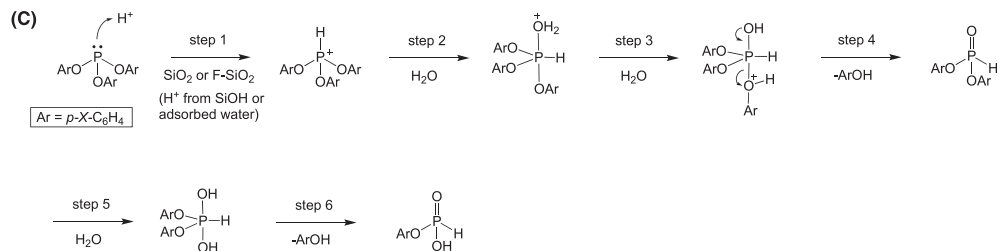
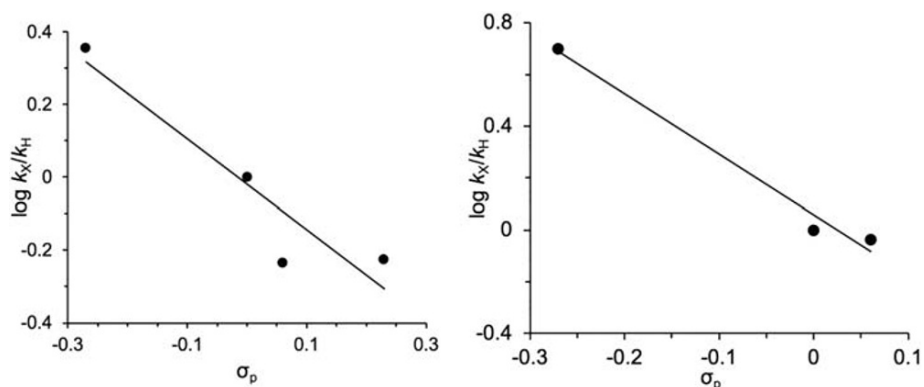


**FIGURE 5** Hammett plots of  $\log k_X/k_H$  vs  $\sigma_p$  for the formation of aryl hydrogen phosphonates **5a–5d** in the hydrolysis of **3a–3d**, respectively on native silica (left plot:  $Y = -1.2465x - 0.02$ ,  $R^2 = 0.8769$ ) and on fluorinated silica (right plot:  $Y = -2.3421x + 0.0564$ ,  $R^2 = 0.9843$ )



The Hammett series of phosphites are susceptible to hydrolysis and influenced by both surface proticity and electronic effects. Proton transfer from ionizable SiOH groups to phosphite can explain why the hydrolysis yield is increased with electron donating substituents, for example, formation of 80% **5a** and 14% **5d** on native silica. Slowing of the hydrolysis reaction is possible by surface fluorination and removal of the SiOH sites and thus dampen the path to aryl hydrogen phosphonate. The

hydrolysis mechanism can be considered, but thought to be improbable by invoking a SiO<sup>-</sup> anion Arbuzov-type rearrangement as was suggested for trimethyl phosphite adsorbed on silica surface,<sup>[23,24]</sup> or a photo-Arbuzov type reaction as seen with phosphites and aryl halides in C–P bond formation.<sup>[25]</sup> Also, we do not invoke chemistry arising from the direct irradiation of the phosphites, as has been reported for phosphines and phosphites, for example with arenediazonium salt reductants,<sup>[26–28]</sup>

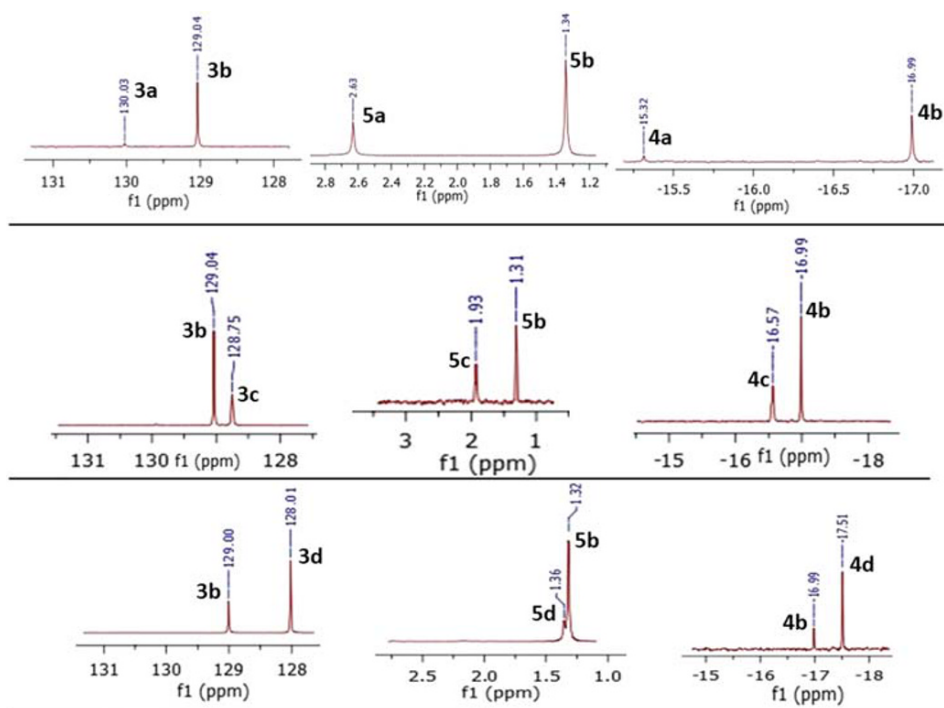


**FIGURE 6** <sup>31</sup>P NMR spectra of **3a–3d**, **4a–4d**, and **5a–5d** in acetonitrile-*d*<sub>3</sub> following their desorption from native silica after a photoreaction of dione **1** and cumylethyl peroxide **2** in the presence of triaryl phosphites **3a–3d**, respectively

**TABLE 3** Proton decoupled  $^{31}\text{P}$  NMR chemical shifts for (*p*-X-C<sub>6</sub>H<sub>4</sub>-O)<sub>3</sub>P **3a-3d**, (*p*-X-C<sub>6</sub>H<sub>4</sub>-O)<sub>3</sub>P=O **4a-4d**, and (*p*-X-C<sub>6</sub>H<sub>4</sub>-O)P(=O)(H)OH **5a-5d**

Compd	( $\delta_{\text{ppm}}$ )	( $\delta_{\text{ppm}}$ )	Compd	( $\delta_{\text{ppm}}$ )	( $\delta_{\text{ppm}}$ )	Compd	( $\delta_{\text{ppm}}$ )	( $\delta_{\text{ppm}}$ )	Compd	( $\delta_{\text{ppm}}$ )	( $\delta_{\text{ppm}}$ )
<b>3a</b>	130.0	129.3 <sup>a</sup>	<b>3b</b>	129.0	128.0 <sup>a</sup>	<b>3c</b>	128.8	127.8 <sup>a</sup>	<b>3d</b>	128.0	127.0 <sup>a</sup>
<b>4a</b>	15.3	-15.6 <sup>a</sup>	<b>4b</b>	-17.0	-17.0 <sup>a,b</sup>	<b>4c</b>	-16.6	-16.6 <sup>a</sup>	<b>4d</b>	-17.5	-17.5 <sup>a</sup>
<b>5a</b>	2.6	NA	<b>5b</b>	1.3	1.3 <sup>c-f</sup>	<b>5c</b>	1.9	NA	<b>5d</b>	1.4	NA

<sup>a</sup>Ref. 53.<sup>b</sup>Ref. 58.<sup>c</sup>Ref. 17.<sup>d</sup>Ref. 59.<sup>e</sup>Ref. 60.<sup>f</sup>Ref. 61.

which can undergo one-electron oxidation to radical cations and couple with oxygen, or in aryl phosphites with P–O cleavage to reach a triplet aryl cation and hydrogen phosphonate.<sup>[29]</sup> In our case, dione **1** is selectively irradiated and sensitizes the homolysis of **2** to reach alkoxy radicals in an oxygen-free environment. Our vessel was degassed with N<sub>2</sub> so that photooxidation chemistry is unavailable, as was observed for phosphine–<sup>1</sup>O<sub>2</sub> reactions to form dioxaphosphorane intermediates<sup>[30,31]</sup> or via radical cation peroxy species with electron-poor sensitizers, such as 9,10-dicyanoanthracene.<sup>[32,33]</sup>

Our results suggest a give-and-take where protonation enhances the conversion of (*p*-X-C<sub>6</sub>H<sub>4</sub>-O)<sub>3</sub>P (a modest antioxidant) to *p*-X-C<sub>6</sub>H<sub>4</sub>-OH (a superior antioxidant) depending on electronics and surface effects. Along these lines, in previous studies of the oxidation of alkyl phosphites,<sup>[12]</sup> (MeO)<sub>3</sub>P is reactive with alkoxy radicals, but its hydrolysis product MeOH is modest antioxidant requiring ~0.5 M concentrations to intercept reactive oxygen species.<sup>[34]</sup> Unlike alkyl alcohols, phenolic compounds have high antioxidant potencies and thus are often used in tenths or single digit millimolar concentrations, such as in 5-amino salicylic acid<sup>[35]</sup> and butylated hydroxytoluene (BHT).<sup>[36]</sup> In terms of our system for alkoxy radical photogeneration at the air/solid interface, it bears some resemblance to surface-bound photochemical<sup>[37–39]</sup> and sensitization reactions,<sup>[40,41]</sup> and selective photooxidation chemistry,<sup>[42–48]</sup> although usually in porous media unlike our current study on nonporous nanoparticles.

## 4 | CONCLUSION

Surface-bound radicals can be challenging to study, and yet are prevalent on atmospheric particles and biological surfaces. Despite progress with EPR,  $^{31}\text{P}$  NMR and phosphite traps can offer advances to the field, as is demonstrated here. Our results demonstrate that triaryl

phosphites **3a-3d** undergo alkoxy radical oxidation, chelation, and hydrolysis on silica nanoparticles by different mechanisms. These mechanisms are summarized in Figure 1 (paths A-C).

Despite relatively few reports,<sup>[49–51]</sup> the sensitized homolysis of an organic peroxide is used here to provide a facile source of alkoxy radicals. In our case, cumyloxy and ethoxy radicals are generated and react with (*p*-F-C<sub>6</sub>H<sub>4</sub>-O)<sub>3</sub>P and to a lesser extent (*p*-Cl-C<sub>6</sub>H<sub>4</sub>-O)<sub>3</sub>P suggesting that these alkoxy radicals do not efficiently acquire H-atoms from surface SiOH groups or surface-adsorbed water. However, the surface proticity can readily catalyze the hydrolysis of more electron rich phosphites, such as **3a**, thereby releasing of *p*-substituted phenols. Interestingly, this opens up the possibility for studying increases in antioxidant power as phenols release from their phosphites.

Future work can include an exploration of the radical scavenging ability of phenols *p*-X-C<sub>6</sub>H<sub>4</sub>-OH compared to the steric BHT-type phenolic antioxidants. Furthermore, sensitized peroxide homolysis experiments for RO• •OR' to reach chain-terminated (scrambled) ROOR and R'OR' products could provide a means to assess the radical migratory aptitude on the nanoparticles.

## 5 | EXPERIMENTAL

### 5.1 | General

The following reagents were purchased from Sigma Aldrich and used as received: hydrophilic fumed silica nanoparticles (200–300 nm diameter, 200 ± 25 m<sup>2</sup>/g surface area), 4,4'-dimethylbenzil **1**, cumene hydroperoxide, ethyl bromide, (PhO)<sub>3</sub>P **3b**, 4-methoxyphenol, *p*-cresol, 4-fluorophenol, 4-chlorophenol, phosphorous trichloride, trimethoxy(3,3,4,4,5,5,6,6,6-nonafluorohexyl)silane, tetra-*N*-butylammonium bromide (TBAB), KOH, NaOH, MgSO<sub>4</sub>, pyridine, cyclohexane, and diethyl ether. The

following solvents were purchased from VWR and used as received: acetonitrile, acetonitrile-*d*<sub>3</sub>, chloroform-*d*, methanol, dichloromethane, and hexanes.

## 5.2 | Synthesis of cumylethyl peroxide 2

Cumylethyl peroxide **2** is a known compound and was synthesized using a literature procedure.<sup>[52]</sup> Briefly, KOH (6 mmol, 0.673 g), phase-transfer catalyst (TBAB, 0.3 mmol, 0.010 g), and cumene hydroperoxide (3 mmol, 0.456 g) were stirred in cyclohexane (3.0 mL) at 50°C for 30 min. Then, a solution of ethyl bromide (3 mmol, 0.222 mL, 0.327 g) in cyclohexane (2 mL) was added and the reaction stirred at 50°C for 4 h. Afterward, by-product KBr was filtered off and the reaction mixture poured into a separatory funnel and the cyclohexane layer separated. The cyclohexane layer was washed with 5% aqueous NaOH, and then washed with water three times. The solution was dried over MgSO<sub>4</sub>, after which the cyclohexane was evaporated at reduced pressure to afford **2**. The <sup>1</sup>H NMR spectrum (Figure S2) showed the presence of impurities, in which an HPLC trace (Figure S3) pointed to 82% purity of **2** based on its relative peak area to those of side-products, such as cumene hydroperoxide and cumyl alcohol. Upon weighing the sample with an analytical balance and considering the 82% purity, a 74% yield of **2** is calculated. An external standard was not used in calculating the percent yield. <sup>1</sup>H NMR (400 MHz, CDCl<sub>3</sub>) δ 7.55 – 7.48 (m, 3H), 7.38 – 7.35 (m, 2H), 4.01 (q, *J* = 7.0 Hz, 2H), 1.63 (s, 6H), 1.18 (t, *J* = 7.0 Hz, 3H).

## 5.3 | Synthesis of tris(4-*X*-phenyl) phosphites [X = MeO (**3a**), F (**3c**), and Cl (**3d**)]

Phosphites **3a**, **3c**, and **3d** are known and were synthesized using a literature procedure<sup>[53]</sup> in 40%, 27%, and 64% yields, respectively. The percent yields were determined after purification by column chromatography and weighing of the dried compounds on an analytical balance. The <sup>1</sup>H NMR spectra did not show the presence of impurities, and thus the percent purities of phosphites **3a**, **3c**, and **3d** were estimated to be ~99%. Briefly, to a solution of 19.6 mmol *p*-substituted phenol and 25 mmol pyridine in 20 mL diethyl ether was added dropwise 5.0 mmol phosphorus trichloride at 0°C under a N<sub>2</sub> atmosphere. Then the reaction mixture was stirred under N<sub>2</sub> at 25°C for 1.5 h, and subsequently quenched with water. The diethyl ether phase was separated, washed with water and brine, dried over MgSO<sub>4</sub>, and concentrated under reduced pressure. The residue for each sample was

purified by silica gel column chromatography using 4:1 dichloromethane-hexanes as an eluent to afford phosphites **3a**, **3c**, and **3d**, each as a colorless viscous oil.

## 5.4 | Silica preparation

Fluorinated fumed silica was prepared based on a method we previously reported,<sup>[54]</sup> which is similar to other reports.<sup>[55,56]</sup> Hydrophilic fumed silica nanoparticles (0.41 g) were placed into a 30 mL toluene solution of trimethoxy(3,3,4,4,5,5,6,6,6-nonafluorohexyl) silane (18 mmol, 6.62 g) and refluxed for 24 h under a N<sub>2</sub> atmosphere. The loading of the fluorosilane to the surface by siloxane bonds was approximately 1.45 mmol/g of silica, where any fluorosilane not covalently bound to the particles was removed by Soxhlet extraction with methanol. Compounds were adsorbed to native and fluorinated silica in a manner previously reported.<sup>[51,57]</sup> In subdued room light, 4,4'-dimethylbenzil **1** (0.01 mmol), cumylethyl peroxide **2** (0.1 mmol), and triaryl phosphites **3a-3d** (pairs of them each 0.1 mmol) were dissolved in 5 mL dichloromethane and stirred with 1.0 g of native silica or fluorinated silica particles for 1 h in a 25 mL round bottom flask. The dichloromethane was evaporated from the particles with a stream of N<sub>2</sub> gas and then by applying a vacuum. The percent loading of adsorbed sensitizer **1**, peroxide **2**, and phosphites **3a-3d** was calculated to be 0.7%, 7%, and 7%, respectively (equations 1-5). Equation 1 gives the number of silanol groups per gram of native silica as the commercial sample contains about 4 silanol groups/nm<sup>2</sup>. Equation 2 shows the number of moles of silanol per gram of silica by dividing number of silanol, obtained in equation 1, with Avogadro's number 6.0221367 × 10<sup>23</sup> mol<sup>-1</sup> (N<sub>A</sub>). Dividing the moles of **1** or **2** or **3a-3d** with moles of silanol groups in equation 2, give the percent loading of each via equations 3, 4, and 5, respectively.

$$\text{Number of silanol/g of SiO}_2 = 200 \times (\text{number of silanol/m}^2) \quad (1)$$

$$\text{Moles of silanol/g of native silica} = \frac{200 \times (\text{number of silanol/m}^2)}{N_A} \quad (2)$$

$$\% \text{loading of } \mathbf{1} = \frac{\text{moles of } \mathbf{1}}{\text{moles of silanol/g of SiO}_2} \quad (3)$$

$$\% \text{loading of } \mathbf{2} = \frac{\text{moles of } \mathbf{2}}{\text{moles of silanol/g of SiO}_2} \quad (4)$$

$$\% \text{loading of phosphite } \mathbf{3a-3d} = \frac{\text{moles of } \mathbf{3a-3d}}{\text{moles of silanol/g of SiO}_2} \quad (5)$$

Adsorbed compounds are assumed to be dispersed homogeneously on the silica nanoparticle surfaces.

Expected loading is on the outer layer of the particles as there is no pores in these fumed silica samples. No special precautions were used to remove physisorbed water.

## 5.5 | Photolysis and heating

A cylindrical vial (20 cm<sup>3</sup>) containing native or fluorinated silica particles (200 mg) adsorbed with **1**, **2**, and pairs of phosphites (e.g., **3a** and **3b**, **3b** and **3c**, or **3b** and **3d**) was N<sub>2</sub>-degassed. This container was attached to a stirring paddle and irradiated with a metal-halide lamp (280 < λ < 700 nm) or heated for 1 h, in which the silica particles were tumbling. Compounds were then desorbed from the silica surfaces with acetonitrile, and the acetonitrile solution delivered through a syringe filter to separate the silica off, evaporated with reduced pressure, and the residue dissolved in acetonitrile-*d*<sub>3</sub> for measurements with <sup>31</sup>P and <sup>1</sup>H NMR.

## 5.6 | Compound detection by <sup>31</sup>P and <sup>1</sup>H NMR

The aryl phosphites **3a-3d**, aryl phosphates **4a-4d**, and aryl hydrogen phosphonates **5a-5d** were detected by <sup>31</sup>P NMR (Figure 6 and Table 3). <sup>31</sup>P NMR for **5b** at δ1.30 ppm is similar with the literature value ranging between 1.08-1.4 ppm.<sup>[17,59-61]</sup> The proton-decoupled <sup>31</sup>P peaks for **3a**, **3b**, **3c**, and **3d** appeared at 130, 129, 128.7, and 128 ppm, respectively, agreed well with (±) 0.04 - (±)1.0 ppm values that were previously reported.<sup>53</sup> Peaks at 2.60, 1.94, and 1.36 ppm were assigned to aryl hydrogen phosphonates **5a**, **5c**, and **5d**, respectively. For example, on fluorinated silica, the percent yield of **4c** was calculated from the peak areas, **4c**/(**3c** + **4c** + **5c**) = 0.52/(1 + 1.13 + 0.52) = 20%; the percent yield of **5c** was calculated from the peak areas, **5c**/(**3c** + **4c** + **5c**) = 1.13/(1 + 1.13 + 0.52) = 42%. <sup>1</sup>H NMR peaks for phosphites **3a-3d** are also reported in the literature.<sup>[53]</sup> The <sup>1</sup>H NMR data of **3a** showed two sets of doublets for aromatic protons that were found at 6.86 ppm (*J* = 8 Hz, 6 H) and 7.07 ppm (*J* = 8 Hz, 6 H). In addition to the twelve aromatic protons, nine methoxy protons for **3a** appeared at 3.81 ppm as a singlet. <sup>1</sup>H NMR data show for aromatic protons, two sets of doublet or multiplet was found for all phosphites except **3c**. For **3c**, a multiplet for 12H appeared within 7.11-7.01 ppm. Twelve aromatic protons came as two sets of multiplets within 7.33-7.29 ppm and 7.08-7.04 ppm for **3d**.

## ACKNOWLEDGEMENT

National Science Foundation, Grant/Award Number: CHE-1856765. We thank Leda Lee for the graphic arts work.

## ORCID

Alexander Greer  <https://orcid.org/0000-0003-4444-9099>

## REFERENCES

- [1] M. D. E. Forbes, S. R. Ruberu, K. E. Dukes, *J. Am. Chem. Soc.* **1994**, *116*, 7299.
- [2] M. D. E. Forbes, K. E. Dukes, T. L. Myers, H. D. Maynard, C. S. Breivogel, H. B. Jaspán, *J. Phys. Chem.* **1991**, *95*, 10547.
- [3] M. D. E. Forbes, L. E. Jarocha, S. Sim, V. F. Tarasov, *Adv. Phys. Org. Chem.* **2013**, *47*, 1.
- [4] E. Vejerano, S. Lomnicki, B. Dellinger, *Environ. Sci. Technol.* **2011**, *45*, 589.
- [5] L. Khachatryan, E. Vejerano, S. Lomnicki, B. Dellinger, *Environ. Sci. Technol.* **2011**, *45*, 8559.
- [6] H. Truong, S. Lomnicki, B. Dellinger, *Environ. Sci. Technol.* **2010**, *44*, 1933.
- [7] B. Dellinger, W. A. Pryor, R. Cueto, G. L. Squadrito, V. Hegde, W. A. Deutsch, *Chem. Res. Toxicol.* **2001**, *14*, 1371.
- [8] B. A. DeHaven, J. T. Tokarski, A. A. Korous, F. Mentink-Vigier, T. M. Makris, A. M. Brugh, M. D. E. Forbes, J. van Tol, C. R. Bowers, L. S. Shimizu, *Chem. – Eur. J.* **2017**, *23*, 8315.
- [9] F. Szocs, M. Klimova, I. Chodak, I. Chorvath, *Eur. Polym. J.* **1996**, *32*, 401.
- [10] A. J. Carrasquillo, K. E. Daumit, J. H. Kroll, *J. Phys. Chem. Lett.* **2015**, *6*, 2388.
- [11] J. J. Orlando, G. S. Tyndall, T. J. Wallington, *Chem. Rev.* **2003**, *103*, 4657.
- [12] S. J. Belh, N. Walalawela, S. Lekhtman, A. Greer, *ACS Omega* **2019**, *4*, 22623.
- [13] J. C. Tebby, *Organophosphorus Chem.* **2009**, *38*, 64.
- [14] F. H. Osman, F. A. El-Samahy, *Monatsh. Chem.* **2007**, *138*, 973.
- [15] F. H. Osman, F. A. El-Samahy, *Chem. Rev.* **2002**, *102*, 629.
- [16] M. R. Mahran, W. M. Abdou, M. D. Khidre, *Monatsh. Chem.* **1990**, *121*, 51.
- [17] W. Oberhauser, G. Manca, *Inorg. Chem.* **2018**, *57*, 4824.
- [18] W. D. Habicher, I. Bauer, J. Pospisil, *Macromol. Symp.* **2005**, *225*, 147.
- [19] B. P. Roberts, *Chem. Soc. Rev.* **1999**, *28*, 25.
- [20] C. V. Lundgren, A. L. Koner, M. Tinkl, U. Pischel, W. M. Nau, *J. Org. Chem.* **2006**, *71*, 1977.
- [21] M. Salamone, M. Bietti, *Acc. Chem. Res.* **2015**, *48*, 2895.
- [22] J. Fossey, D. Lefort, J. Sorba, *Free Radicals in Organic Chemistry*, John Wiley & Sons, New York **1995** 53.
- [23] I. D. Gay, A. J. McFarlan, B. A. Morrow, *J. Phys. Chem.* **1991**, *95*, 1360.
- [24] A. K. Bhattacharya, G. Thyagarajan, *Chem. Rev.* **1981**, *81*, 415.
- [25] R. S. Shaikh, S. J. S. Düsel, B. König, *ACS Catal.* **2016**, *6*, 8410.
- [26] S. Yasui, S. Yamazaki, *J. Phys. Org. Chem.* **2020**, e4021.
- [27] S. Yasui, T. Ando, M. Ozaki, Y. Ogawa, K. Shioji, *Heteroat. Chem.* **2018**, *29*, e21468.
- [28] S. Yasui, M. R. Badal, S. Kobayashi, M. Mishima, *J. Phys. Org. Chem.* **2014**, *27*, 967.

- [29] M. Terpolilli, D. Merli, S. Protti, V. Dichiarante, M. Fagnoni, A. Albini, *Photochem. Photobiol. Sci.* **2011**, *10*, 123.
- [30] D. G. Ho, R. Gao, J. Celaje, H.-Y. Chung, M. Selke, *Science* **2003**, *302*, 259.
- [31] N. Sawwan, A. Greer, *Chem. Rev.* **2007**, *107*, 3247.
- [32] S. M. Bonesi, S. Protti, A. Albini, *J. Org. Chem.* **2016**, *81*, 11678.
- [33] S. M. Bonesi, S. Protti, A. Albini, *J. Org. Chem.* **2018**, *83*, 8104.
- [34] M. Hoffman, A. Rajapakse, X. Shen, K. S. Gates, *Chem Res. Toxicology* **2012**, *25*, 1609.
- [35] T. C. P. Dinis, V. M. C. Madeira, L. M. Almeida, *Arch. Biochem. Biophys.* **1994**, *315*, 161.
- [36] H. Li, X. Zhou, P. Gao, Q. Li, H. Li, R. Huang, M. Wu, *Anim. Nutr.* **2016**, *2*, 234.
- [37] T. Hasegawa, M. Imada, M. Yoshioka, *J. Phys. Org. Chem.* **1993**, *6*, 494.
- [38] Y. S. Liu, P. de Mayo, W. R. Ware, *J. Phys. Chem.* **1993**, *97*, 5987.
- [39] P. de Mayo, K. Okada, M. Rafalska, A. C. Weedon, G. S. K. Wong, *Chem. Commun.* **1981**, *16*, 820.
- [40] V. Ramamurthy, J. Sivaguru, *Chem. Rev.* **2016**, *116*, 9914.
- [41] N. Walalawela, A. Greer, Remote Singlet Oxygen Delivery Strategies, in *Singlet Oxygen: Applications in Biosciences and Nanosciences*, (Eds: S. Nonell, C. Flors), Royal Society of Chemistry, London. **2016**, 335.
- [42] E. Ramasamy, N. Jayaraj, M. Porel, V. Ramamurthy, *Langmuir* **2012**, *28*(1), 10.
- [43] A. Natarajan, L. S. Kaanumalle, S. Jockusch, C. L. Gibb, B. C. Gibb, N. J. Turro, V. Ramamurthy, *J. Am. Chem. Soc.* **2007**, *129*, 4132.
- [44] J. Sivaguru, H. Saito, M. R. Solomon, L. S. Kaanumalle, T. Poon, S. Jockusch, W. Adam, V. Ramamurthy, Y. Inoue, N. J. Turro, *Photochem. Photobiol.* **2006**, *82*, 123.
- [45] G. C. Vougioukalakis, Y. Angelis, J. Vakros, G. Panagiotou, C. Kordulis, A. Lycourghiotis, M. Orfanopoulos, *Synlett.* **2004**, *6*, 971.
- [46] J. Vakros, G. Panagiotou, C. Kordulis, A. Lycourghiotis, G. C. Vougioukalakis, Y. Angelis, M. Orfanopoulos, *Catalysis Lett.* **2003**, *89*, 269.
- [47] M. Warrier, N. J. Turro, V. Ramamurthy, *Tetrahedron Lett.* **2000**, *41*, 7163.
- [48] E. L. Clennan, J. P. Sram, *Tetrahedron Lett.* **1999**, *40*, 5275.
- [49] J. C. Scaiano, G. G. Wubbels, *J. Am. Chem. Soc.* **1981**, *103*, 640.
- [50] B. K. Shah, A. Gusev, M. A. J. Rodgers, D. C. Neckers, *J. Phys. Chem. A* **2004**, *108*, 5926.
- [51] N. Walalawela, A. Greer, *J. Phys. Org. Chem.* **2018**, e3807.
- [52] S. Baj, A. Siewniak, *Appl. Catal. A* **2010**, *385*, 208.
- [53] M. Oba, Y. Okada, K. Nishiyama, W. Ando, *Org. Lett.* **2009**, *11*, 1879.
- [54] D. Bartusik, D. Aebisher, G. Ghosh, M. Minnis, A. Greer, *J. Org. Chem.* **2012**, *77*, 4557.
- [55] R. Campos, A. J. Guenther, T. S. Haddad, J. M. Mabry, *Langmuir* **2011**, *27*, 10206.
- [56] I. M. El-Nahhal, N. M. El-Ashgar, *J. Organomet. Chem.* **2007**, *692*, 2861.
- [57] S. Fioressi, R. Arce, *Environ. Sci. Technol.* **2005**, *39*, 3646.
- [58] M. Weber, C. Hellriegel, A. Rueck, J. Wuethrich, P. Jenks, M. Obkircher, *Anal. Bioanal. Chem.* **2015**, *407*, 3115.
- [59] S. B. Tzokov, R. T. Momtcheva, N. G. Vassilev, J. Kaneti, D. D. Petkov, *J. Am. Chem. Soc.* **1999**, *121*, 5103.
- [60] J. Jankowska, M. Sobkowski, J. Stawinski, A. Kraszewski, *Tetrahedron Lett.* **1994**, *35*, 3355.
- [61] A. Kers, I. Kers, J. Stawinski, M. Sobkowski, A. Kraszewski, *Tetrahedron* **1996**, *52*, 9931.

## SUPPORTING INFORMATION

Additional supporting information may be found online in the Supporting Information section at the end of this article.

**How to cite this article:** Ghosh G, Greer A. A fluorinated phosphite traps alkoxy radicals photogenerated at the air/solid interface of a nanoparticle. *J Phys Org Chem.* 2020;e4115. <https://doi.org/10.1002/poc.4115>